A New Mechanism for Mendelian Dominance in Regulatory Genetic Pathways: Competitive Binding by Transcription Factors

Adam H. Porter,*,†,1 Norman A. Johnson,*,† and Alexander Y. Tulchinsky†,‡

*Department of Biology and †Graduate Program in Organismic and Evolutionary Biology, University of Massachusetts Amherst, Massachusetts 01002 and ‡Department of Biology, State University of New York at New Paltz, New York 12561

ORCID ID: 0000-0002-8154-4207 (A.P.)

ABSTRACT We report a new mechanism for allelic dominance in regulatory genetic interactions that we call binding dominance. We investigated a biophysical model of gene regulation, where the fractional occupancy of a transcription factor (TF) on the *cis*-regulated promoter site it binds to is determined by binding energy ($-\Delta G$) and TF dosage. Transcription and gene expression proceed when the TF is bound to the promoter. In diploids, individuals may be heterozygous at the *cis*-site, at the TF's coding region, or at the TF's own promoter, which determines allele-specific dosage. We find that when the TF's coding region is heterozygous, TF alleles compete for occupancy at the *cis*-sites and the tighter-binding TF is dominant in proportion to the difference in binding strength. When the TF's own promoter is heterozygous, the TF produced at the higher dosage is also dominant. *Cis*-site heterozygotes have additive expression and therefore codominant phenotypes. Binding dominance propagates to affect the expression of downstream loci and it is sensitive in both magnitude and direction to genetic background, but its detectability often attenuates. While binding dominance is inevitable at the molecular level, it is difficult to detect in the phenotype under some biophysical conditions, more so when TF dosage is high and allele-specific binding affinities are similar. A body of empirical research on the biophysics of TF binding demonstrates the plausibility of this mechanism of dominance, but studies of gene expression under competitive binding in heterozygotes in a diversity of genetic backgrounds are needed.

KEYWORDS competitive binding; epistasis; fractional occupancy; genotype–phenotype map; thermodynamics

MENDEL (1866) coined the terms dominant and recessive to describe variants that respectively appear in 3:1 ratios in first-generation hybrid crosses. Wright (1934) proposed a plausible mechanism, demonstrating theoretically that dominance can arise as a natural consequence of functional allelic differences among enzymes that play roles in metabolic pathways. Alleles with reduced function tended to be recessive, and variation in the genetic background could modify the degree of dominance. Kacser and Burns (1981) cast Wright's mechanism into the language of enzyme kinetics and metabolic flux, a mechanism we will call flux dominance, and several studies have extended and modified it (*e.g.*, Keightley and Kacser 1987; Keightley 1996; Bagheri and Wagner 2004). Since then, several other mechanisms have been found to produce dominance, including negative regulatory feedback (Omholt *et al.* 2000), threshold-based reaction-diffusion systems (Gilchrist and Nijhout 2001), protein–protein interactions (Veitia *et al.* 2013), and epigenetic modifications (Li *et al.* 2012; Bond and Baulcombe 2014). In general, dominance arises because the relationship between the genotype and the phenotype it produces is nonlinear (Gilchrist and Nijhout 2001; Veitia *et al.* 2013).

Empirical studies have shown that dominance is commonly found in loci involved in gene regulation. In particular, *trans*-acting alleles [*e.g.*, transcription factors (TFs)] commonly show dominance, whereas alleles of the *cis*-acting sites they regulate only rarely do (Hughes *et al.* 2006; Stupar and Springer 2006; Wray 2007; Li *et al.* 2012; Bond and Baulcombe 2014). The mechanism is unknown. We propose

doi: 10.1534/genetics.116.195255
Manuscript received August 26, 2016; accepted for publication November 4, 2016; published Early Online November 17, 2016.
Supplemental material is available online at www.genetics.org/lookup/suppl/doi:10.1534/genetics.116.195255/-/DC1.
[1]Corresponding author: Morrill Science Center, Room 221, 611 Stockbridge Rd, University of Massachusetts Amherst, Amherst, MA 01003. E-mail: aporter@bio.umass.edu

that this dominance is an inevitable consequence of differences in binding dynamics between *trans*-acting gene products as they compete for access to the *cis*-sites they regulate. The degree of dominance thereby depends on allele-specific differences in concentration and binding affinity of the *trans*-acting allelic variants. Such competitive binding interactions are integral to models of multifactorial gene regulation (Bintu *et al.* 2005b), including nucleosome–TF interactions (Teif *et al.* 2010, 2012), and repressor (Browning and Busby 2004) and microRNA function (Thomson and Dinger 2016), but have not been applied to allelic interactions. This form of Mendelian dominance, which we term binding dominance, propagates through regulatory pathways and is modified by polymorphism at other loci in the pathway. Our findings apply to any *trans*-acting regulatory molecules interacting with *cis*-acting regulatory sites. TF/promoter interactions meet these criteria well and we will develop the model using that language.

Methods

Model overview

Biophysical models have long been used to study molecular interactions between DNA and molecules that bind to it (*e.g.*, Gerland *et al.* 2002; Bintu *et al.* 2005a; Phillips *et al.* 2012; Tulchinsky *et al.* 2014; Khatri and Goldstein 2015). The central premise of these models is that interactions between regulatory molecules and the sites they regulate behave according to the thermodynamic and kinetic principles that drive all molecular interactions. Consistent with empirical data (reviewed in Mueller *et al.* 2013), gene expression in these models only ensues while a TF molecule is physically bound to the promoter of the regulated gene.

In our model, binding is a stochastic process determined by the free energy of association ($-\Delta G$, in units of $1/k_BT$, the Boltzmann constant × the temperature in °K; $-\Delta G$ is negative by definition), between a TF molecule and promoter, which we will call "binding energy." The fractional occupancy θ—the proportion of time a promoter is occupied by a TF molecule, and therefore the gene expression level—depends on $-\Delta G$, and also on dosage [TF], the concentration of free TF molecules available in the nucleus to bind when the promoter is unoccupied.

The biophysical model represents interacting TF molecules and the promoter sequence as strings of bits of arbitrary length (Figure 1A), an approach based in statistical physics and information theory (Gerland *et al.* 2002). This method of abstraction permits characterization of molecular interactions at arbitrary scales, from the state space of electrostatic interaction among atoms to amino acid and nucleotide variation, and ultimately, to the genetic basis of variation in those molecules. The binding energy decays to 0 in steps of $-\Delta G_1$ as m, the proportion of mismatched bits over the length of the bitstring, increases (Teif *et al.* 2010). Specifically, m is the Hamming distance between the bitstrings, scaled to the bitstring length (Figure 1A). The binding energy is related to the dissociation constant K as $K = \exp[-\Delta G]$. Here, we present the model at the physiological scale, in terms of [TF] and K, which may be more accessible to readers. Its analog at the scale of physically interacting molecules is presented in Supplemental Material, File S1. The haploid model, a parameter-reduced form of our model in Tulchinsky *et al.* (2014) (see File S1), is

$$\theta = \frac{[TF]/(\Delta K)^m}{1 + [TF]/(\Delta K)^m} \tag{1}$$

where $\Delta K = \exp[-\Delta G_1]$ is the stepwise change in the dissociation constant, such that $K = (\Delta K)^m$.

We use the following notational conventions throughout. Interacting loci are labeled with letters A and B, with C included for three-locus pathways. Subscripts indicate allelic variants as in Figure 1, panels B and C; those before the letter (*e.g.*, $_1$A) refer to promoter alleles and those after the letter (*e.g.*, A_1) indicate coding region alleles (therefore, TF structural variants). Subscripts are dropped for homozygotes (*e.g.*, AA), and both subscripts are used when both sites vary for an allele (*e.g.*, $_1A_1$ and $_2A_2$). Arrows indicate allele-specific regulatory interactions, *e.g.*, $m_{A1\rightarrow 1B}$ represents bitstring mismatches between TF allele A_1 and *cis*-site allele $_1$B. We use brackets for concentration, *e.g.*, [TF] represents the concentration of a generic TF with $[TF]_{sat}$ as its saturating concentration, and $[A_1]$ represents the concentration of the TF structural variant coded by allele copy 1 of locus A.

Diploid model

In diploids, TF variants A_1 and A_2 (Figure 1B) compete for occupancy at both promoter sites $_1$B and $_2$B independently (Tulchinsky *et al.* 2014) and the concentration of TF molecules is the sum of those from each TF allele copy, *i.e.*, $[A_1] + [A_2] = [TF]$. Under TF competition, the fractional occupancy of A_1 on promoter site $_1$B in the presence of A_2 is

$$\theta_{A1\rightarrow 1B} = \frac{[A_1]/(\Delta K)^{m_{11}}}{1 + \frac{[A_1]}{(\Delta K)^{m_{11}}} + \frac{[A_2]}{(\Delta K)^{m_{21}}}} \tag{2a}$$

where m_{11} ($= m_{A1\rightarrow 1B}$) and m_{21} ($= m_{A2\rightarrow 1B}$) are the proportions of mismatches between the bit strings of A_1 and A_2 to that of $_1$B, respectively (see File S1). Fractional occupancies of the other three interactions are calculated analogously,

$$\theta_{A2\rightarrow 1B} = \frac{[A_2]/(\Delta K)^{m_{21}}}{1 + \frac{[A_1]}{(\Delta K)^{m_{11}}} + \frac{[A_2]}{(\Delta K)^{m_{21}}}} \tag{2b}$$

$$\theta_{A1\rightarrow 2B} = \frac{[A_1]/(\Delta K)^{m_{12}}}{1 + \frac{[A_1]}{(\Delta K)^{m_{12}}} + \frac{[A_2]}{(\Delta K)^{m_{22}}}} \tag{2c}$$

$$\theta_{A2\rightarrow 2B} = \frac{[A_2]/(\Delta K)^{m_{22}}}{1 + \frac{[A_1]}{(\Delta K)^{m_{12}}} + \frac{[A_2]}{(\Delta K)^{m_{22}}}} \tag{2d}$$

where $m_{12} = m_{A1\rightarrow 2B}$ and $m_{22} = m_{A2\rightarrow 2B}$. The final expression level (ϕ) is the sum of the fractional occupancies of the four TF–promoter pairs,

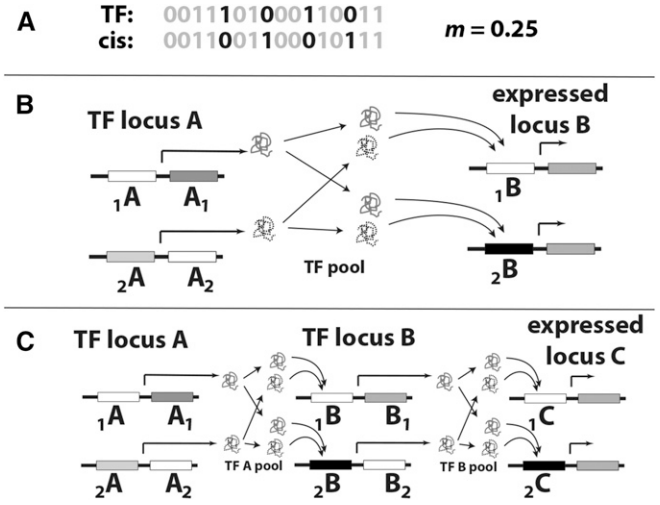

Figure 1 Diploid two- and three-locus regulatory pathways with competitive transcription factor (TF) binding. (A) TF molecules and promoter sites are represented by bitstrings of arbitrary length *n*, and the strength of binding is proportional to the extent of their match; *m* represents the proportion of mismatched bits ($m = h/n$, where h is the Hamming distance), darkened for emphasis. In diploids, each gene copy is assigned a bitstring to each of its variable sites. (B) Two-locus pathway. TF locus A codes for the TF protein that regulates the expressed locus B. Locus A can vary at its own promoter (alleles $_1$A and $_2$A), its coding region (alleles A_1 and A_2), or both; locus B varies only in its promoter ($_1$B and $_2$B). The dosages of each of the TF alleles ($[_1A]$ and $[_2A]$) are determined by their promoter sequences. Subscripts are dropped for homozygotes. (C) Three-locus pathway. As in the two-locus pathway, except that locus B codes for a second TF that goes on to regulate expression of locus C.

$$\phi^* = \frac{1}{2}[(\theta_{A1\rightarrow 1B}+\theta_{A2\rightarrow 1B})+(\theta_{A1\rightarrow 2B}+\theta_{A2\rightarrow 2B})] \qquad (3)$$

where ϕ^* is the unscaled expression. When both TF variants are at saturating concentration, *i.e.*, $[A_1] + [A_2] = [TF]_{sat}$, then maximum fractional occupancy $\theta_{max} = [TF]_{sat}/(1 + [TF]_{sat})$ occurs when $m = 0$, and minimum fractional occupancy $\theta_{min} = [TF]_{sat}/(\Delta K + [TF]_{sat})$ occurs when $m = 1$. We scale expression to the range [0,1] using $\phi = (\phi^* - \theta_{min})/(\theta_{max} - \theta_{min})$. However, because $\phi < \theta_{min}$ when $m = 1$ and $[TF] < [TF]_{sat}$, we set also set an expression floor at $\phi = 0$, such that

$$\phi = \max\left[\frac{\phi^* - \theta_{min}}{\theta_{max} - \theta_{min}}, 0\right] \qquad (4)$$

This constraint is necessary in the A→B step of the three-locus model described below, and for generality we apply it to both models. As a baseline for scaling purposes, we use TF dosages $[A_1]_{sat} = [A_2]_{sat} = [TF]_{sat}/2$ as the allele-specific saturating concentrations.

Genotype–phenotype (G–P) map

We treat the phenotype, *P*, as being proportional to the expression level of the *cis*-regulated locus, such that $P = \lambda\phi$, and without loss of generality, treat that proportionality constant as $\lambda = 1$, such that $P = \phi$.

In the biophysical model, the bit strings are abstract representations of information content that can characterize underlying genetic differences in the interacting molecules. Equation 1, Equation 2, Equation 3, and Equation 4 therefore characterize the G–P map, the rules by which the phenotype is generated from the underlying genotype as a function of binding energy and TF concentration.

Dominance

Competition between TF alleles for binding to their *cis*-regulated sites creates conditions for allelic dominance (Tulchinsky *et al.* 2014). Following Wright (1934), we use $d = (P_{11} - P_{12})/(P_{11} - P_{22})$ as the dominance coefficient, where P_{12} is the heterozygote phenotype and P_{11} and P_{22} are homozygote phenotypes. Allele "1" of the respective locus is thereby the reference allele for which dominance is assessed. Allele 1 is codominant when $d = 1/2$, completely dominant at $d = 0$, and completely recessive at $d = 1$. When polymorphism occurs at more than one site, these *P*'s represent marginal phenotypes with respect to the reference allele, and *d* is the marginal dominance, holding the rest of the genetic background constant.

If fractional occupancy cannot be measured separately for each allele, then *d* must be assessed phenotypically. Even strong dominance becomes increasingly difficult to detect as ϕ's for homozygotes and heterozygotes of both alleles approach equality because the three genotypes will have very similar phenotypes; the trait will appear to be unaffected by these loci, or the degree of dominance will be obscured by sampling and measurement error. Detectability (*t*) is proportional to the absolute difference between the two homozygote phenotypes, such that $t = \kappa\,|P_{11} - P_{22}|$ with proportionality function κ. In a constant genetic background, κ is some increasing function of the accuracy in the measurement of *P* (or ϕ) and the sample size of the study.

Three-locus pathways: propagation and genetic background

In a linear three-locus pathway (Figure 1C), locus B codes for a second TF that binds to the promoter of locus C, such that there are two regulatory steps, A→B and B→C. The final phenotype is the expression level at locus C ($P = \phi_C$). The promoter and product sites of locus B together comprise a single allele (in this three-locus, two-allele model), and the doubly heterozygous B genotype is denoted $_1B_{12}B_2$. Competitive binding of the A alleles onto the two B alleles proceeds independently, creating two allele-specific expression terms, ϕ_{1B1} and ϕ_{2B2}, based on Equation 2. Expression of these B alleles yields separate $[_1B_1]$ and $[_2B_2]$ values, which we calculate as $[_1B_1] = \phi_{1B1}[B]_{sat}$ and $[_2B_2] = \phi_{2B2}[B]_{sat}$, such that maximal expression of the B locus yields $[_1B_1]_{sat} + [_2B_2]_{sat} = [B]_{sat}$.

Analysis

We considered cases where fractional occupancy and therefore gene expression is maximal ($\phi = P = 1$) when binding is maximal ($m = 0$) and TF concentration is saturating, and that $\phi = P = 0.5$ when $m = 0.5$ at the same $[TF]_{sat}$. Analysis of the

role of TF concentration requires scaling ΔK to $[TF]_{sat}$ in order to meet these constraints. This results in no loss of generality because m is in units of abstract, arbitrarily scalable "information" about properties that affect ΔK in the binding interaction. For example, bits in the TF and *cis*-site bitstrings (Figure 1A) are not intended to correspond one-to-one to single amino acid or nucleotide positions, and stepwise changes in m are not literal representations of substitutions. Rather, the bitstrings are abstract representations of shape and charge, and m informs us of the extent to which they are compatible. Substituting $m = 1/2$ into Equation 2 and Equation 3, and solving Equation 4 for ΔK, we used $\Delta K = [TF]^2_{sat}$.

We report results from the cases where $[TF]_{sat}$ takes the values 10, 100, and 1000. In many cases, we found heterozygote and homozygote phenotypes to be so similar that their differences could be hard to detect in empirical studies. To graphically illustrate the effects of detectability, we overlay the genotype-dominance maps with white opacity masks, grading from opaque at $t = 0$ through translucency to transparency at $t = 1$, where t is the detectability parameter, with the effect of making the underlying genotype-dominance map increasingly visible as t increases. As a heuristic, we treat scaling function κ as a constant arbitrarily set to 4 with a maximum of $t = 1$; *i.e.*, dominance is undetectable when homozygote phenotypes are equal and always detectable when their difference equals or exceeds 1/4.

In three-locus pathways, we used Equation 2 and Equation 4, with appropriate subscripts, to calculate ϕ_C. For simplicity, we assume $[TF]_{sat}$ is the same for both regulatory steps, *i.e.*, $[A]_{sat} = [B]_{sat} = [TF]_{sat}$. All analyses were done using *Mathematica* (Wolfram Research, Inc., 2015) and code used to generate the figures is available on GitHub at https://github.com/adamhporter/Mendelian-dominance-via-transcription-factor-binding.git.

Data availability

The authors state that all data necessary for confirming the conclusions presented in the article are represented fully within the article.

Results

We compare three types of polymorphism (Figure 1B). Polymorphism in the *cis*-regulated B locus is represented as $AA \rightarrow {}_1B_2B$; that in the TF protein-coding region is $A_1A_2 \rightarrow BB$; and variation in TF dosage (*i.e.*, allele-specific [TF] as determined by upstream expression) is ${}_1A_2A \rightarrow BB$. In the three-locus $AA \rightarrow BB \rightarrow CC$ pathway, we consider the propagation and detectability of dominance at locus A with respect to expression at downstream locus C (ϕ_C) and explore genetic background effects when loci B and C are polymorphic or have imperfect binding.

Genotype–phenotype maps

The shapes of the G–P maps differ depending on which site is polymorphic. In the ${}_1A_2A \rightarrow BB$ case (Figure 2, A–C) with maximal TF binding ($m = 0$), ϕ is low when both alleles are at low dosage ([TF]), climbing toward high expression as [TF] of both alleles rises to saturating concentration $[TF]_{sat}$. The effect is very sensitive to $[TF]_{sat}$, such that the region of detectably lower ϕ is confined to the very bottom left corner of Figure 2C when $[TF]_{sat}$ is high. The drop-off in ϕ is proportional to their sum, [TF], therefore perpendicular to the $[{}_1A] = [{}_2A]$ diagonal.

In the $A_1A_2 \rightarrow BB$ case (Figure 2, D–F) at $[TF]_{sat}$, ϕ depends on competitive binding of the TF variants to the *cis*-sites they regulate (Equation 2 and Equation 4). ϕ is high as long as either TF binds tightly ($m_{A1\rightarrow B}$ or $m_{A2\rightarrow B}$ is low), yielding a characteristic L-shaped ridge on the density plot, indicating dominance of the tighter-binding allele. Increasing $[TF]_{sat}$ (Figure 2, E and F) broadens and flattens the ridge.

In the $AA \rightarrow {}_1B_2B$ case (Figure 2, G–I), the expression of the two B-allele copies is additive (Equation 3) and at $[TF]_{sat}$, peak ϕ occurs when both alleles perfectly match the TF ($m_{A\rightarrow 1B} = m_{A\rightarrow 2B} = 0$). Expression falls away on both axes, leaving a characteristic arc on the density plot (Figure 2G), curving opposite the direction of the $A_1A_2 \rightarrow BB$ case. Increasing $[TF]_{sat}$ produces a more plateaued ridge that extends further out along the $m_{A\rightarrow 1B} = m_{A\rightarrow 2B}$ diagonal, visible as a more squared-off arc on the density plot (Figure 2, H and I).

Dominance in expression level ϕ

Dominance at the A locus with respect to ϕ emerges when variation occurs in the TF (the ${}_1A_2A \rightarrow BB$ and $A_1A_2 \rightarrow BB$ cases), with different patterns (Figure 3A–F). However, when variation occurs at the *cis* site (the $AA \rightarrow {}_1B_2B$ case) expression is always codominant ($d = 0.5$; not illustrated) due to the additivity of the products of locus B (Equation 3).

When TF binding varies (the $A_1A_2 \rightarrow BB$ case; Figure 3, A–C), the TF allele with higher binding affinity (lower m) has a competitive advantage and dominant expression. The isoclines follow the diagonal when m is low but flare at higher m such that the competitive binding effect becomes much weaker. In this range, the occupancy of each allele is so low that the TFs effectively cease to compete and the phenotype approaches additivity (*i.e.*, diploid ϕ^* of Equation 3 approaches haploid θ of Equation 1 as m goes to 1). $[TF]_{sat}$ has a strong effect on dominance due to its effect on competition. When $[TF]_{sat}$ is high (Figure 3C), small changes in binding affinity can produce large changes in d, particularly when $m < 0.5$, whereas much larger changes in m are required for the same effect at $[TF]_{sat} = 10$ (Figure 3A). Polymorphism in the B locus has no effect on the dominance of A_1 in the $A_1A_2 \rightarrow {}_1B_2B$ case.

When TF dosage varies (the ${}_1A_2A \rightarrow BB$ case; Figure 3, D–F), the allele with higher [TF] is dominant. The isoclines spread linearly from the bottom left corner of the density plot, where [TF] is low for both alleles, continuing into the region beyond the dotted line where total TF concentration is saturating ($[{}_1A] + [{}_2A] \geq [TF]_{sat}$). This dominance pattern is not substantially altered by $[TF]_{sat}$, nor is it by $m < 1$ provided that the TF coding region and the *cis*-site are homozygous. These plots are therefore not shown.

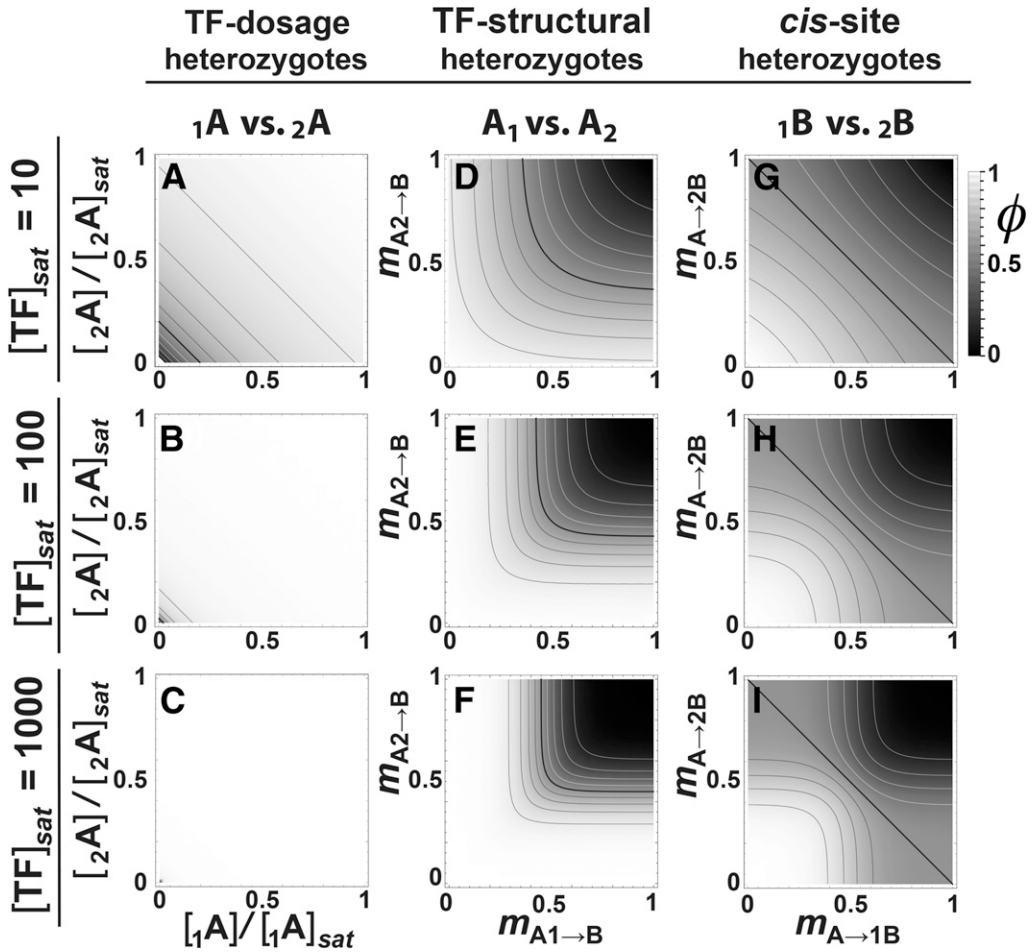

Figure 2 Genotype–phenotype maps in the two-locus regulatory pathway with competitive transcription factor (TF) binding. Genotype–phenotype maps, shown as density plots of expression level (ϕ), equivalent to phenotype in this model ($\phi = P$). Rows: Three saturating TF concentrations ($[TF]_{sat}$) at maximal binding ($m_{A1\rightarrow B} = m_{A2\rightarrow B} = 0$). (A–C) Effects of allelic variation in TF dosage, scaled to allele-specific $[TF]_{sat}$. (D–F) Effects of allelic variation in the TF coding region expressed as mismatch (m) with a homozygous *cis*-site promoter BB. (G–I) Effects of allele-specific variation in the *cis*-site, holding the TF homozygous. Isoclines throughout represent intervals of 0.1 and the black isocline represents $\phi = 0.5$.

When TF dosage and binding affinity both vary (the ${}_1A_1{}_2A_2 \rightarrow$ BB case), the two sources of dominance interact cooperatively. Figure 3H shows the effect of allelic variation $[{}_1A_1]$ and $[{}_2A_2]$ under conditions where $m_{A1\rightarrow B} = 0.1$, $m_{A2\rightarrow B} = 0.2$, and $[TF]_{sat} = 100$. For orientation, Figure 3H represents the effects of varying dosage [TF] for the binding strength combination lying at the position of the circle in Figure 3B; the circles in the centers of Figure 3B and Figure 3H represent the same conditions. At this saturating concentration (*i.e.*, $[A_1]_{sat} = [A_2]_{sat} = [TF]_{sat}/2$ at both circles), allele ${}_1A_1$ is dominant with $d = 0.291$. Along the *x*-axis in Figure 3H, increasing the dosage of the more tightly binding ${}_1A_1$ allele above $[A_1]_{sat}$ increases its dominance, whereas decreasing its concentration pushes d back toward codominance until dominance is ultimately reversed and ${}_1A_1$ becomes recessive. Along the *y*-axis, increasing the dosage of the ${}_2A_2$ allele also counteracts dominance of the ${}_1A_1$ allele, but the rate of change is much slower, and is only able to reverse the direction of dominance if $[A_1]$ and $[A_2]$ start well below $[TF]_{sat}/2$.

Dominance is more sensitive to binding affinity than to differences in dosage. Figure 3G reflects the same conditions as Figure 3E but with a fivefold difference in allele-specific dosages, $[A_1] = [TF]_{sat}/2$ and $[A_2] = [TF]_{sat}/10$. For orientation, the orange crosses in Figure 3, E and G share common parameter settings. Under these maximum-binding conditions, ${}_1A_1$ is dominant with $d = 0.17$. In Figure 3G, codominance is restored when binding of ${}_1A_1$ is reduced by ~20%, becoming recessive beyond that.

Detectability of dominance in the phenotype

Figure 4 shows the dominance maps of Figure 3, A–F overlaid by white opacity masks that obscure d in proportion to the similarity of the expression levels in homozygotes. Existing dominance due to dosage differences in the ${}_1A_2A \rightarrow$ BB case is likely to be hard to detect unless $[TF]_{sat}$ is low and the dosages differ strongly (Figure 4D), and is likely to be detectable only in loss-of-expression alleles when $[TF]_{sat}$ is high (Figure 4, E and F). Detectability is higher in the $A_1A_2 \rightarrow$ BB case, especially when $[TF]_{sat}$ is low (Figure 4A). As $[A]_{sat}$ increases (Figure 4, B and C), the region of low detectability of dominance broadens in the high- and low-expression regions of the corresponding G–P maps (Figure 2E and Figure 3F).

Three-locus pathways

Using a three-locus linear pathway (Figure 1C), we assessed the G–P maps and the dominance of the dosage (${}_1A$) and binding (A_1) sites with respect to expression of locus C (ϕ_C). We will call this dominance d_{AC}. We also examined the effects of genetic background by varying binding in the B→C step.

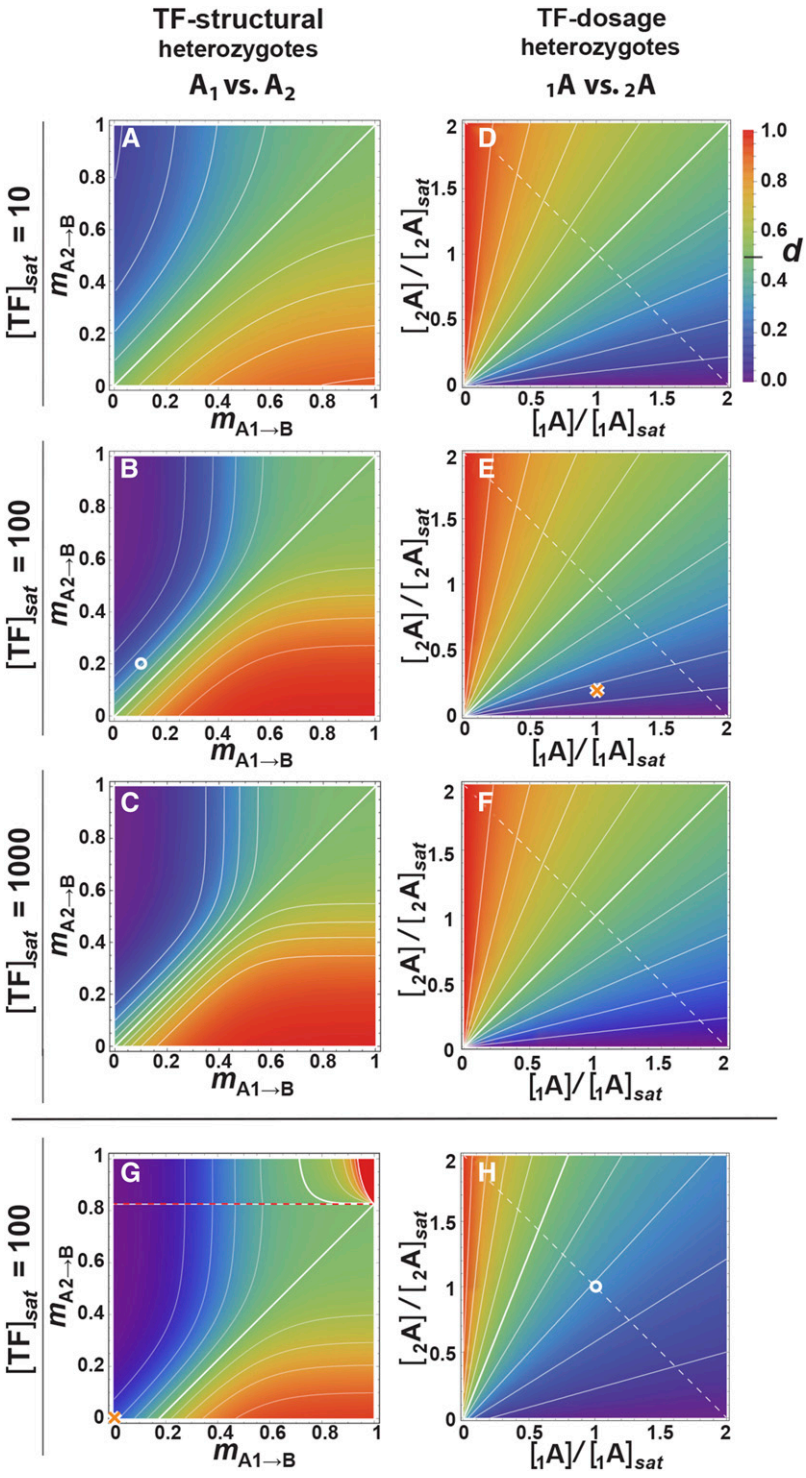

Figure 3 Genotype-dominance maps, shown as density plots. Dominance (*d*) is with respect to the reference transcription factor (TF) allele A_1 (or $_1A$); that allele is dominant in the blue region and recessive in the red. Dominance is symmetrical, so where A_1 is recessive, A_2 is dominant. (A–C) $A_1A_2 \rightarrow BB$ cases: dominance at the TF coding region. *d* as a function of the degree of mismatch (*m*) between a homozygous *cis* site and competing TF-coding alleles A_1 and A_2, for three saturating TF concentrations ($[TF]_{sat}$); the tighter-binding allele (low *m*) is dominant. The circle in 3B has the same *m* and [TF] values as the circle in (H). (D–F) $_1A_2A \rightarrow BB$ cases: dominance in TF dosage. *d* as a function of expression level of the two TF alleles $_1A$ and $_2A$, expressed as a fraction of the saturating TF dosage ($[TF]_{sat}$). TF dosage is saturating ($[_1A] + [_2A] \geq [TF]_{sat}$) above the dotted diagonal line. The higher-dosage TF is dominant. (G and H) $_1A_{12}A_2 \rightarrow BB$ cases. (G) Dominance as a function of the degree of mismatch in the heterozygous genetic background where TF alleles differ in dosage, for the case where $[_1A] = [TF]_{sat}/2$ and $[_2A] = [TF]_{sat}/10$. The orange crosses in this and (E) have the same *m* and [TF] values. Above the dotted line at $m_{A2\rightarrow B} = 0.82552$, $\phi_{aa} = 0$ for the $_2A_2$ homozygote and $d = (\phi_{AA}-\phi_{Aa})/\phi_{AA}$, marking a discontinuity on the map. (H) Effect of allele-specific concentration in TF in a heterozygous genetic background, where the TF's coding region is heterozygous ($m_{1A1\rightarrow B} = 0.1$, $m_{2A2\rightarrow B} = 0.2$, $[TF]_{sat} = 100$). The circle has the same *m* and [TF] values as the circle in (B). Isoclines throughout represent intervals of 0.1 and the thicker white isocline denotes $d = 0.5$.

The G–P map of the TF-dosage case (the $_1A_2A \rightarrow BB \rightarrow CC$ case) with $[TF]_{sat} = 10$ (Figure 5A) is a steeper version of the $_1A_2A \rightarrow BB$ map (Figure 2A), such that ϕ_C is nearly maximal unless [A] is very low for both A alleles. Higher values of $[TF]_{sat}$ yield such steep G–P maps at low dosage that only virtual double-knockout $_1A_2A$ genotypes are able to appreciably reduce locus C's expression (not illustrated). The G–P map for the TF-binding case (the $A_1A_2 \rightarrow BB \rightarrow CC$ case; Figure 5B shows $[TF]_{sat} = 10$) takes the same general form as the $A_1A_2 \rightarrow BB$ map (Figure 3E), but has a broad, high-expression plateau such that far greater $A \rightarrow B$ mismatch is required for an equivalent reduction of ϕ_C. At higher $[TF]_{sat}$ (not illustrated), the region of low expression becomes increasingly confined to the top right corner such that only very weak $A \rightarrow B$ binding affects ϕ_C at maximal $B \rightarrow C$ binding. The plateau becomes even broader and the

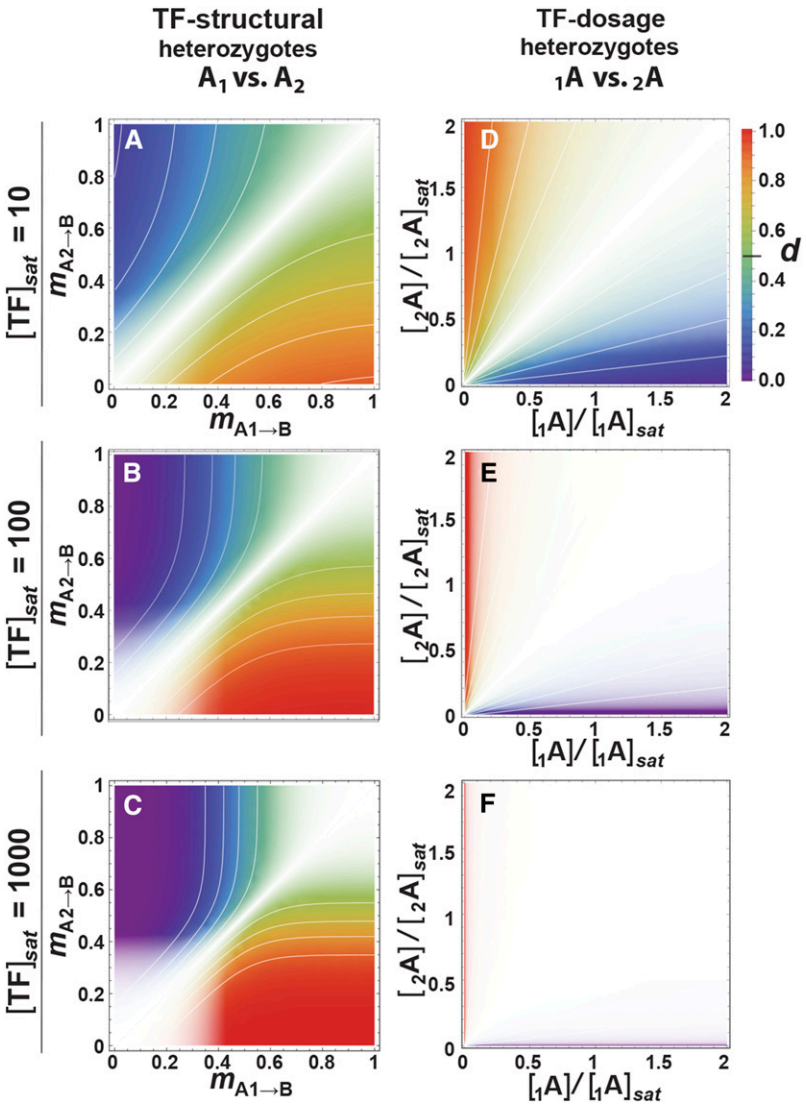

Figure 4 Detectability of dominance with respect to genotype. White opacity-gradient masks overlay the genotype-dominance maps of the corresponding panels of Figure 3, A–F, such that the intensity of underlying color represents the detectability of dominance. Isoclines throughout represent intervals of 0.1. TF, transcription factor.

shape squares off as it does for the $A_1A_2 \rightarrow BB$ maps of Figure 3, D–F.

Dominance at the $_1A$ and A_1 sites propagates down the pathway to yield dominance with respect to ϕ_C. In the $A_1A_2 \rightarrow BB \rightarrow CC$ case, the transition of d_{AC} from dominant to recessive lies parallel to the $m_{A1\rightarrow B} = m_{A2\rightarrow B}$ diagonal when $m_{B\rightarrow C} = 0$ (Figure 5C and Figure 6A), and increasing $[TF]_{sat}$ steepens the transition (Figure 5D and Figure 6B). d_{AC} is weaker and more sensitive to binding strength when $m_{B\rightarrow C} = 0.5$ but is slightly more detectable (Figure 6, C and D). d_{AC} drops rapidly between $0.5 \leq m_{B\rightarrow C} \leq 1$ and becomes very hard to detect, especially when $[TF]_{sat}$ is high (not shown). Here, without sensitive assays of expression, even unexpressed, completely recessive A alleles may go undetected.

Despite the differences in their G–P maps, dominance in the $_1A_2A \rightarrow BB \rightarrow CC$ case is almost identical to that of the $_1A_2A \rightarrow BB$ case seen in Figure 3, D–F. However, its detectability (Figure 7, A–F) is much weaker (*e.g.*, compare Figure 4D to Figure 7A). It increases slightly when $m_{B\rightarrow C} = 0.5$ (Figure 7C), but drops to become negligible beyond that (not shown). For higher levels of $[TF]_{sat}$, dominance will only be detectable when one of the A alleles is unexpressed (Figure 7, B and D) unless assays are extremely sensitive.

Polymorphism in the genetic background can modify d_{AC}, but the magnitude of the effect depends on the background type. The effect is greatest in the $_1A_2A \rightarrow {}_1B_2B \rightarrow CC$ case, where dosage differences in TF locus A coexist with binding site variation in the *cis* site of locus B. For illustration, we've chosen a combination where dosage of the $_1A$ allele is maximal ($[_1A] = [TF]_{sat}/2$) and that of the $_2A$ allele is low ($[_2A] = [TF]_{sat}/10$), at the position of the square in Figure 7A, such that dominance is strong and relatively easy to detect. Figure 6G shows the effect of binding variation in the A→B step, due to variation in the B-locus promoter ($m_{A\rightarrow 1B}$ *vs.* $m_{A\rightarrow 2B}$; the coding region of TF A is monomorphic) at this dosage combination. As overall A→B binding decreases ($m_{A\rightarrow B}$ increases), d_{AC} increases (and becomes more detectable) until, ultimately, allele $_1A$ becomes recessive. This effect is less pronounced as $[TF]_{sat}$ increases (Figure 6H), and also as the dosage differences decrease (not shown). Discontinuities in

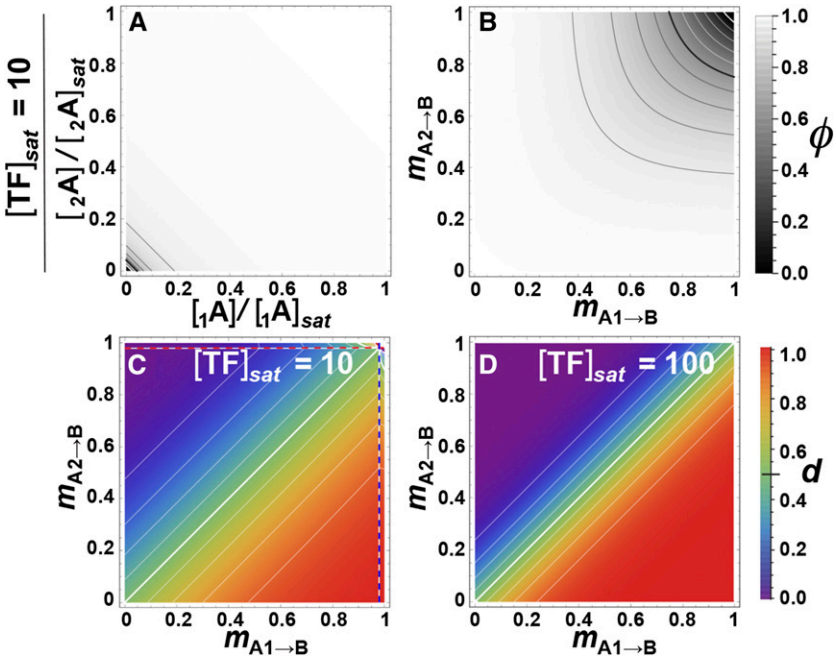

Figure 5 Downstream effects of dominance in the three-locus pathway: dominance of locus A with respect to expression at locus C. (A and B) Genotype–phenotype maps with $[TF]_{sat} = 10$. (C and D) Genotype-dominance maps of $A_1A_2 \rightarrow BB \rightarrow CC$, with $m_{B \rightarrow C} = 0$. (C) The dotted lines mark discontinuities: at high $m_{A1 \rightarrow B}$ beyond the blue dotted line, $\phi_{AA} = 0$ for the A_1A_1 homozygote such that $d = \phi_{Aa}/\phi_{aa}$; at high $m_{A2 \rightarrow B}$ above the red dotted line, $\phi_{aa} = 0$ for the A_2A_2 homozygote such that $d = (\phi_{AA}–\phi_{Aa})/\phi_{AA}$; beyond both lines in the top right corner, d is undefined. Isoclines throughout represent intervals of 0.1. TF, transcription factor.

the isoclines of Figure 6, G and H, shown as dashed lines, are explained in Figure S1.

Other foreground/background combinations have weaker effects or none at all, and they mostly affect detectability. In Figure 6, E and F, we show an example for the $A_1A_2 \rightarrow B_1B_2 \rightarrow CC$ case, where the genetic background consists of a high-functioning B_1 allele ($m_{B1 \rightarrow C} = 0$) and a low-functioning B_2 allele ($m_{B2 \rightarrow C} = 0.9$). Detectability is somewhat higher relative to the $A_1A_2 \rightarrow BB \rightarrow CC$ cases (Figure 6, panels A and B, respectively) but the effect on d_{AC} is negligible. In the ${}_1A_2A \rightarrow B_1B_2 \rightarrow CC$ case, detectability of d_{AC} is largely determined by the dominant B allele in the $B \rightarrow C$ step, such that the genotype-dominance maps (not shown) are virtually indistinguishable from the ${}_1A_2A \rightarrow BB \rightarrow CC$ cases of Figure 7, A and B. There is no effect on d_{AC} of variation in the C-locus promoter (the $A_1A_2 \rightarrow BB \rightarrow {}_1C_2C$ and ${}_1A_2A \rightarrow BB \rightarrow {}_1C_2C$ cases; not illustrated), but it reduces detectability by reducing ϕ_C.

Discussion

We find that dominance emerges in regulatory genetic pathways due to competitive molecular interactions between TF variants in heterozygotes as they bind to their shared promoters. Alleles with higher competitive ability are inevitably dominant with respect to their contributions to fractional occupancy. However, between *cis*-acting alleles, dominance cannot occur because the corresponding transcripts are independently expressed, such that overall expression is their sum. Dominance effects extend to expression of downstream loci in multi-step pathways, and polymorphism therein can generate genetic background effects. However, this form of dominance is likely to be phenotypically detectable only when TF dosages or binding strengths are in the range where overall gene expression levels differ measurably between homozygotes. We discuss each of these properties and their implications.

Binding dominance: a new mechanism for Mendelian dominance

Competition occurring between allelic TF variants for binding to the promoter sites they regulate (Equation 2; the $A_1A_2 \rightarrow BB$ and ${}_1A_2A \rightarrow BB$ interactions) represents a novel mechanism of dominance at the molecular level. The strength of the dominance depends on the biophysical properties of the interaction between TF molecules and the promoter sites to which they bind. When TF variants differ in their binding affinities ($-\Delta G$), the variant with higher affinity is dominant (Figure 3, A–C). Dominance of the competing TF variants is also sensitive to TF availability ([TF]; Figure 3, D–F). This is because, when [TF] is low, fractional occupancy is likewise low and there is little competition at the binding site; the allelic effects approach additivity. Conversely, at high [TF], the more abundant TF allele more often occupies the promoter sequence, driving expression in the heterozygote. In contrast, polymorphism at the downstream *cis*-regulatory site ($AA \rightarrow {}_1B_2B$) cannot contribute to dominance. This is because expression of the *cis*-regulated gene product, or respectively the TF variant, proceeds independently for each allele and overall expression is their sum. In the three-locus pathway, dominance in locus A can propagate down the pathway, such that A alleles can show dominance with respect to expression of locus C (ϕ_C; Figure 5, C and D, Figure 6, and Figure 7) as well as locus B (ϕ_B).

Binding dominance differs from the type of dominance that arises in metabolic pathways, which we call *flux dominance*, though the mechanisms of both are rooted in the biophysics of molecular interactions. In enzymes embedded in metabolic

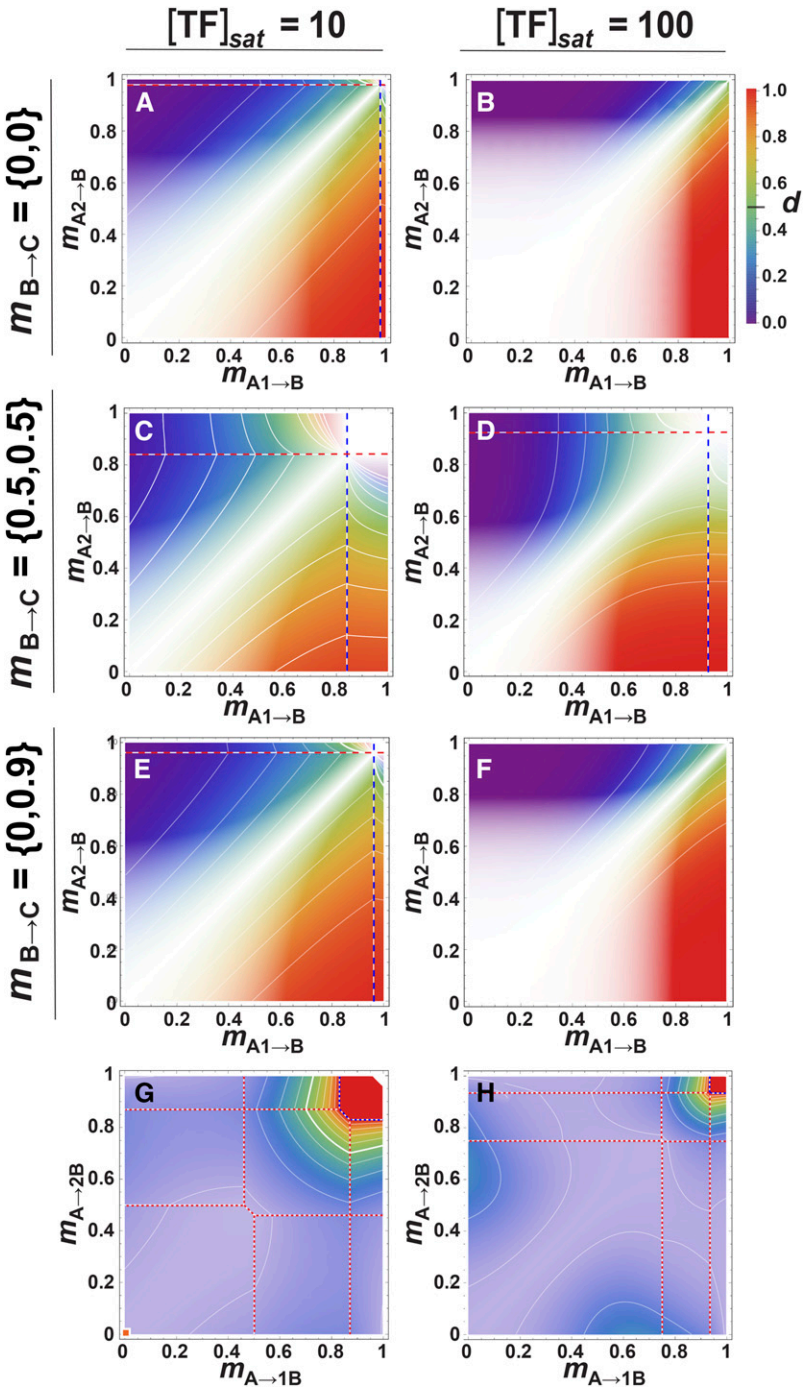

Figure 6 Genetic background effects on dominance in the three-locus pathway. Pattern and detectability of d at the coding site of transcription factor (TF) locus A in the three-locus pathway with respect to expression at downstream locus C (ϕ_C), when TF locus B varies in its coding site. White opacity-gradient masks overlay the genotype-dominance maps, proportionally obscuring regions of low detectability. Notation: $m_{B\rightarrow C} = \{x,y\}$ means that $m_{B1\rightarrow C} = x$ and $m_{B2\rightarrow C} = y$; locus B is homozygous when $x = y$. (A–F) Effects of varying binding in the B→C interaction by changing the coding site of the B-locus's TF. The dotted lines mark discontinuities: at high $m_{A1\rightarrow B}$ beyond the blue dotted line, $\phi_{AA} = 0$ for the A_1A_1 homozygote such that $d = \phi_{A1A2}/\phi_{A2A2}$; at high $m_{A2\rightarrow B}$ above the red dotted line, $\phi_{aa} = 0$ for the A_2A_2 homozygote such that $d = (\phi_{AA}-\phi_{Aa})/\phi_{AA}$; beyond both lines in the top right corner, d is undefined. (G and H) Effects of changing the B-locus promoter region in the ${}_1A_2A \rightarrow {}_1B_2B \rightarrow CC$ case, with detectability overlays. Low binding in the A→B step reverses the dominance pattern due to dosage differences of the A alleles. (G) $m_{A\rightarrow 1B}$ *vs.* $m_{A\rightarrow 2B}$; $[TF]_{sat} = 10$, $[{}_1A] = [TF]_{sat}/2$, $[{}_2A] = [TF]_{sat}/10$. The orange square at the origin represents the same parameter conditions as the orange square in Figure 7A; *i.e.*, (G) represents a projection from Figure 7A taken at a point where the dosage of the ${}_1A$ allele is maximal and that of the ${}_2A$ allele is very low. The dotted lines separate regions where the expression levels of either or both alleles of locus B (ϕ_{1B} and ϕ_{2B}) equal 0 in the genotypes ${}_1A_2A$ and ${}_2A_2A$. Those combinations are shown in Figure S1. (H) Same, but with $[TF]_{sat} = 100$. Isoclines throughout represent intervals of 0.1.

pathways, dominant alleles have higher rates of catalysis (k_{cat}), thus producing a higher flux from substrate to product, and the degree of dominance is proportional to the difference in k_{cat} values (Kacser and Burns 1981; Keightley and Kacser 1987; Keightley 1996). Flux dominance is sensitive to substrate saturation of the enzyme (Bagheri-Chaichian *et al.* 2003), analogous to the way $[TF]_{sat}$ affects the degree of binding dominance through fractional occupancy. Flux dominance does not explain the effects of mutations at regulatory loci (Keightley 1996) because regulatory genetic pathways do not experience flux.

Protein assembly dominance occurs when some subunits of complex proteins are expressed in inappropriate concentrations or have defective structures, disrupting the stoichiometry of protein assembly (Veitia 2003; Veitia *et al.* 2013). These represent downstream effects in the binding-dominance model, where subunit concentrations are determined by allele-specific ϕ_{1B1} and ϕ_{2B2}, the expression levels of the B_1 and B_2 structural variants. The phenotype has a nonlinear relationship to gene expression, or in our notation, $P = k\phi$ becomes $P = k(\phi_{1B1}, \phi_{2B2})$, where k is now a function of the expression levels and binding properties of the other subunits in the complex.

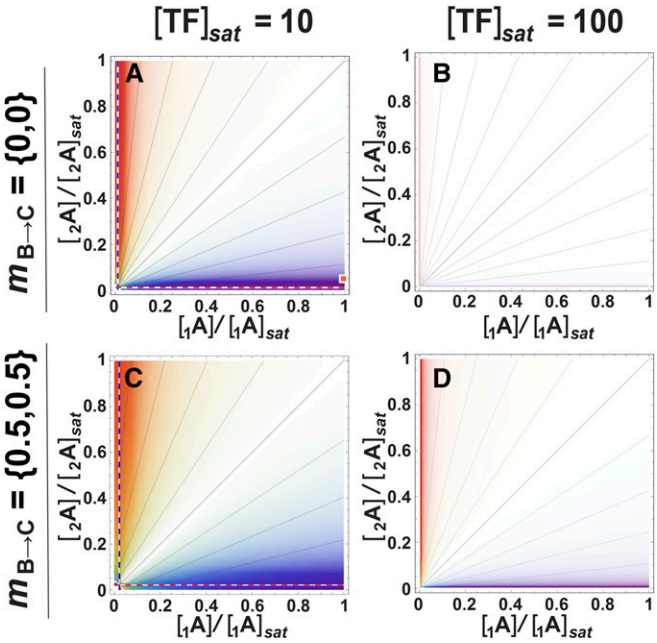

Figure 7 Pattern and detectability of dominance of allele-specific concentration differences of TF locus A in the three-locus pathway, in relation to saturating TF concentration and binding strength in the B→C step. (A–D) White opacity-gradient masks overlay the genotype-dominance maps, proportionally obscuring regions of low detectability. Notation: $m_{B\rightarrow C} = \{x,y\}$ means that $m_{B1\rightarrow C} = x$ and $m_{B2\rightarrow C} = y$; locus B is homozygous when $x = y$. (A) The orange square represents the same parameter conditions as the orange square in Figure 6G, *i.e.*, Figure 6G examines genetic background effects on dominance at a point where the $_1$A allele has maximal dosage and the dosage of the $_2$A allele is very low. Isoclines throughout represent intervals of 0.1.

Feedback dominance results from cases where a gene product autoregulates its expression. Omholt *et al.* (2000) analyzed feedback dominance using the biophysically relevant Hill (1910) equation, which permits serially repeated promoter site sequences; they considered only cases that lacked polymorphism in the TF coding region. Gene products could regulate either their own promoters (in our notation, $_1A_2A\rightarrow {}_1A_2A$) or the promoters of an upstream TF ($_1A_2A\rightarrow {}_1B_2B\rightarrow {}_1A_2A$). These pathways resemble the $_1A_2A\rightarrow {}_1B_2B$ and $_1A_2A\rightarrow {}_1B_2B\rightarrow$ CC cases for which we find dominance, suggesting that feedback dominance may ultimately prove to be a special case of binding dominance. To our knowledge, the effects of polymorphism in the coding regions, thus competitive binding, on feedback dominance remain unexplored.

Diffusion dominance arises in network-based regulation of ontogenetic diffusion gradients, including morphogen concentrations, their diffusion and decay rates, and the threshold concentrations necessary to initiate a phenotypic response (Gilchrist and Nijhout 2001). Allelic variation affecting any of these components can show dominance in network output. While we have presented our model in the context of TF–promoter interactions, its principles apply broadly to interactions between any genetically determined, interacting regulatory molecules. Our simple regulatory pathways represent elements in these more complex diffusion-based networks, and we expect that dominance due to competitive binding will be inherent in them.

Detectability and cryptic dominance

Biophysical conditions that lead to especially high or low fractional occupancies, determining respectively the bottom left and top right corners of the G–P maps (Figure 2 and Figure 5, A and B), can mask dominance because the two homozygotes have very similar phenotypes. This can occur when m is similar for both alleles, or when allele-specific dosage [TF] is either high enough to saturate the binding site, or low enough that the binding site is rarely occupied by either allele. Even strong dominance at the level of molecular interactions can remain cryptic (*e.g.*, compare Figure 3, D–F to Figure 4, D–F). When $[TF]_{sat}$ is high, only completely unexpressed $_1$A or $_2$A alleles will be detectable as recessive (Figure 4, E and F) and moderate to strong dominance will likely go undetected. Likewise, when both TF alleles have similar binding affinities or dosages, the alleles will be nearly codominant, lying along the region of the diagonals of Figure 3, A–F, but all individuals will also have nearly identical phenotypes. There, even polymorphism will be difficult to detect without genotyping; the degree of dominance may be of little practical importance in these cases anyway. Nevertheless, we predict that cryptic dominance will become apparent in assays of allele-specific expression levels (Mueller *et al.* 2013) in association with dosage and binding strength variation.

Detectability of dominance in the three-locus pathway (Figure 6 and Figure 7) is lower than in the two-locus pathway (Figure 4), because detectability is successively attenuated when it passes through [TF] of downstream loci. In the three-locus pathway, the A→B step determines [B]. In general, [TF] must be low for differences in [TF] to affect expression (Figure 3, A–C; this is also why low detectability is widespread in the $_1A_2A\rightarrow$ BB case of Figure 4, D–F). It takes relatively large changes in expression in the A→B step to appreciatively change [B], and therefore to detect differences in expression at loci further downstream.

Effects of genetic background

Polymorphism in the genetic background can enhance, obscure, or even reverse binding dominance. There are two types of background effects in the two-locus regulatory interaction and several more in the three-locus pathway. In the two-locus pathway, dominance of coding site (A_1 and A_2) alleles at the TF locus is unaffected by polymorphism in the *cis*-regulated locus (*i.e.*, $d_{A1A2\rightarrow 1B2B} = d_{A1A2\rightarrow BB}$). However, when allele-specific TF dosages and binding affinities ([TF] and m) are permitted to vary in the $_1A_{12}A_2\rightarrow$ BB case, dominance of coding site TF variants is affected by polymorphism in their promoters (Figure 3G) and vice versa (Figure 3H). For a given TF coding region (A_1A_2) heterozygote, dominance modification is asymmetrical, being more effective when the dosage of the tighter-binding A allele is varied (Figure 3H). In contrast, for a given dosage ($_1A_2A$) heterozygote, changes in binding

affinities of either allele have effects of similar magnitude (Figure 3G).

In the three-locus pathway, detectability of d_{AC} is further modified by binding strength in the B→C step, such that it is least attenuated when $m_{B\to C} = 0.5$ (for $[TF]_{sat} = 10$, compare Figure 6, A and C and also Figure 7, A and C; for $[TF]_{sat} = 100$, compare Figure 6, B and D and also Figure 7, B and D). This is where the G–P map for the B-locus TF coding region is steepest (Figure 2, D–F), therefore where $|\phi_{C.11}-\phi_{C.22}|$ (the denominator of d_{AC}) is greatest. d_{AC} becomes almost undetectable when $m_{B\to C}$ is high because G–P maps are nearly flat there (Figure 2, D–F), such that the underlying two-locus dominance is nearly undetectable (Figure 4, B and C). Polymorphism at the coding site of locus B (the $A_1A_2\to B_1B_2\to$CC and $_1A_2A\to B_1B_2\to$CC cases) modifies detectability only negligibly (Figure 6, G and H and Figure 7, G and H), because expression at the B→C step incorporates dominance of the tighter-binding allele. Modifying binding strength $m_{B\to C}$ by changing the C-locus promoter has the same effect on d_{AC} as does changing the B-locus coding region, but does not affect dominance in the BB→$_1C_2$C case because expression there is additive.

Flux dominance is similarly sensitive to allelic substitutions that occur up to several steps removed along a metabolic pathway (Kacser and Burns 1981; Keightley 1996). Bagheri-Chaichian *et al.* (2003) show that the downstream dominance effects are sensitive to enzyme saturation at intermediate steps, much as we see in binding site saturation in regulatory pathways (Figure 6 and Figure 7). Feedback dominance likewise shows downstream effects (Omholt *et al.* 2000) in pathways with the structure $_1A_2A\to BB\to$($_1A_2A$ and CC), *i.e.*, where the product of locus B coregulates a downstream locus C as well as an upstream locus A. In this case, dominance of the A_1 allele is detectable in the expression of locus C. Omholt *et al.* (2000) did not directly assess attenuation of the signal due to saturation at intermediate steps; rather, they noticed and excluded it by considering only cases where homozygotes showed differences >25%.

Binding dominance is likely to interact with flux dominance. When locus B codes for a metabolic enzyme, flux dominance of allele B_1 can be modified in $_1A_2A\to B_1B_2$ or $A_1A_2\to B_1B_2$ interactions, provided that regulatory changes in B's expression levels affect enzyme saturation in the three B-locus genotypes. Polymorphism in both the promoter and product site of the B locus, *i.e.*, the $_1A_2A\to{}_1B_{12}B_2$ and $A_1A_2\to{}_1B_{12}B_2$ cases, should further influence B_1's flux dominance by further changing relative allozyme concentrations. Conversely, we expect changes in allozyme concentration or k_{cat} due to variation in $_2$B or B_2 to modify, mask, or expose binding dominance at $_1$A or A_1 when d_{A1} is assessed using genotype-specific fluxes in the metabolic pathway.

Beyond the regulatory pathway, TFs interact with other molecules in the cell that may be influenced by genetic background. These include direct interactions with proteins that regulate TF availability, spurious DNA, RNA, or protein binding, and indirect effects of physiological conditions such as pH (Mueller *et al.* 2013). These affect the $[TF]/[TF]_{sat}$ ratio but have negligible effect on dominance and its detectability: the isoclines of Figure 3, D–F and the detectability gradients of Figure 4, D–F are linear, therefore constant with respect to this ratio. However, dominance may be modified in cases where TF variants differ in their responses to the nonspecific background or are regulated differently (*i.e.*, A_1A_2 cases with properties closer to the $_1A_{12}A_2$ case). For analytical convenience in this study, these secondary binding effects are subsumed into [TF] (see parameter reduction in File S1). The unreduced model of Tulchinsky *et al.* (2014) may be necessary in the design and interpretation of experiments.

Empirical studies

Consistent with the competitive binding model, *cis*-site heterozygotes typically show additive expression whereas *trans* heterozygotes commonly show dominance (Wray 2007; Guo *et al.* 2008; Tirosh *et al.* 2010; Zhang *et al.* 2011; Gruber *et al.* 2012; Meiklejohn *et al.* 2014), although some *cis*-site polymorphisms show patterns of dominance as well (Guo *et al.* 2008; Lemos *et al.* 2008). Our modeling suggests the possibility that unidentified polymorphism in regulatory loci upstream, in disequilibrium with the *cis* site, may be involved in at least some of these exceptions. Motifs with variable numbers of binding site repeats in the promoter region could also potentially produce binding dominance and even overdominance, as they do in feedback dominance (Omholt *et al.* 2000).

Mueller *et al.* (2013) review empirical work on the biophysics of fractional occupancy in regulatory interactions. Gene expression is highly correlated with fractional occupancy of TFs on their binding sites, as our model assumes. Site-specific mutagenesis, using a variety of techniques for measuring binding affinity at primary *vs.* secondary (likely to be spurious background) binding sites, reveals strong differences in binding affinity among artificial promoter region alleles ($_1$B and $_2$B alleles, in our notation). Some of these techniques are themselves based on measures of competitive binding among sites. Gaur *et al.* (2013) review studies demonstrating that TF and promoter region alleles show significant patterns of allele-specific gene expression in diverse model organisms. Nevertheless, to our knowledge, allelic variation in TF binding affinity and concentration, in diverse genetic backgrounds, with respect to its effects on competitive binding and heterozygote gene expression, remain to be studied.

Concluding remarks

In the discovery and documentation of regulatory architectures that drive gene expression, it has been necessary and appropriate to use inbred lines and careful breeding designs in model organisms to control for heterozygosity and to homogenize the genetic background. Outside of the laboratory, polymorphism is ubiquitous. Our understanding of gene regulation must account for it as we learn to predict and manipulate gene expression in the face of multilocus heterozygosity and,

ultimately, as we design and implement new regulatory architectures, in diverse systems of importance in medical, agricultural, and fundamental research. A comprehensive, quantitative, and mechanistically robust theory of Mendelian dominance will likely be required, and binding dominance is likely to be a significant component of it.

Acknowledgments

We thank C. Babbitt and anonymous reviewers for valuable comments on the manuscript, and J. Birchler for an enjoyable and insightful conversation.

Literature Cited

Bagheri, H. C., and G. P. Wagner, 2004 Evolution of dominance in metabolic pathways. Genetics 168: 1713–1735.

Bagheri-Chaichian, H., J. Hermisson, J. R. Vaisnys, and G. P. Wagner, 2003 Effect of epistasis on phenotypic robustness in metabolic pathways. Math. Biosci. 184: 27–51.

Bintu, L., N. E. Buchler, H. G. Garcia, U. Gerland, T. Hua *et al.*, 2005a Transcriptional regulation by the numbers: models. Curr. Opin. Genet. Dev. 15: 116–124.

Bintu, L., N. E. Buchler, H. G. Garcia, U. Gerland, T. Hua *et al.*, 2005b Transcriptional regulation by the numbers: applications. Curr. Opin. Genet. Dev. 15: 125–135.

Bond, D. M., and D. C. Baulcombe, 2014 Small RNAs and heritable epigenetic modification in plants. Trends Cell Biol. 24: 100–107.

Browning, D. F., and S. J. W. Busby, 2004 The regulation of bacterial transcription initiation. Nat. Rev. Microbiol. 2: 1–9.

Gaur, U., K. Li, S. Mai, and G. Liu, 2013 Research progress in allele-specific expression and its regulatory mechanisms. J. Appl. Genet. 54: 271–283.

Gerland, U., J. D. Moroz, and T. Hwa, 2002 Physical constraints and functional characteristics of transcription factor-DNA interaction. Proc. Natl. Acad. Sci. USA 99: 12015–12020.

Gilchrist, M. A., and H. F. Nijhout, 2001 Nonlinear developmental processes as sources of dominance. Genetics 159: 423–432.

Gruber, J. D., K. Vogel, G. Kalay, and P. J. Wittkopp, 2012 Contrasting properties of gene-specific regulatory, coding, and copy number mutations in *Saccharomyces cerevisiae*: frequency, effects, and dominance. PLoS Genet. 8: e1002497.

Guo, M., S. Yang, M. Rupe, B. Hu, D. R. Bickel *et al.*, 2008 Genome-wide allele-specific expression analysis using massively parallel signature sequencing (MPSS) reveals *cis*- and *trans*-effects of gene expression in maize hybrid meristem tissue. Plant Mol. Biol. 66: 551–563.

Hill, A. V., 1910 The possible effect of the aggregation of the molecules of hemoglobin. J. Physiol. 40: iv–viii.

Hughes, K. A., J. F. Ayroles, M. M. Reedy, J. M. Drnevich, K. C. Rowe *et al.*, 2006 Segregating variation in the transcriptome: *cis* regulation and additivity of effects. Genetics 173: 1347–1355.

Kacser, H., and J. A. Burns, 1981 The molecular basis of dominance. Genetics 97: 639–666.

Keightley, P. D., 1996 A molecular basis for dominance and recessivity. Genetics 143: 621–625.

Keightley, P. D., and H. Kacser, 1987 Dominance, pleiotropy and metabolic structure. Genetics 117: 319–329.

Khatri, B. S., and R. A. Goldstein, 2015 A course-grained model of sequence evolution and the population size dependence of the speciation rate. J. Theor. Biol. 378: 56–64.

Lemos, B., L. O. Araripe, P. Fontanillas, and D. L. Hartl, 2008 Dominance and the evolutionary accumulation of *cis*- and *trans*-effects on gene expression. Proc. Natl. Acad. Sci. USA 105: 14471–14476.

Li, Y., K. Varala, S. P. Moose, and M. P. Hudson, 2012 Inheritance pattern of 24 nt siRNA clusters in Arabidopsis hybrids is influenced by proximity to transposable elements. PLoS One 7(10): e47043.

Meiklejohn, C. D., J. D. Coolon, D. L. Hartl, and P. J. Wittkopp, 2014 The roles of *cis*- and *trans*-regulation in the evolution of regulatory incompatibilities and sexually dimorphic gene expression. Genome Res. 24: 84–95.

Mendel, G. J., 1866 Versuche über Pflanzen-Hybriden. Verhandlungen der naturforschenden Vereins in Brunn. 4: 3–47. Reprinted as Experiments in plant hybridization (in English) on MendelWeb, Ed. 97.1, edited by R. B. Blumberg. Available at: http://www.mendelweb.org/Mendel.html. Accessed: July 5, 2016.

Mueller, F., T. J. Stasevich, D. Maza, and J. D. McNally, 2013 Quantifying transcription factor kinetics: at work or at play? Crit. Rev. Biochem. Mol. Biol. 48: 492–514.

Omholt, S. W., E. Plahte, L. Øyehaug, and K. Xian, 2000 Gene regulatory networks generating the phenomena of additivity, dominance and epistasis. Genetics 155: 969–990.

Phillips, R., J. Kondev, J. Thierot, and H. Garcia, 2012 *Physical Biology of the Cell*, Ed. 2. Garland Science, New York.

Stupar, R. M., and N. M. Springer, 2006 *Cis*-transcriptional variation in maize inbred lines B71 and Mo17 leads to additive expression patterns in the F_1 hybrid. Genetics 173: 2199–2210.

Teif, V. B., R. Ettig, and K. Rippe, 2010 A lattice model for transcription factor access to DNA. Biophys. J. 99: 2597–2607.

Teif, V. B., A. V. Shkrabkou, V. P. Egorova, and V. I. Krot, 2012 Nucleosomes in gene regulation: theoretical approaches. Mol. Biol. 46: 1–10.

Thomson, D. W., and M. E. Dinger, 2016 Endogenous microRNA sponges: evidence and controversy. Nat. Rev. Genet. 17: 273–283.

Tirosh, I., S. Reikhav, N. Segal, Y. Assia, and N. Barkai, 2010 Chromatin regulators as capacitors of interspecies variations in gene expression. Mol. Syst. Biol. 6: 435.

Tulchinsky, A. Y., N. A. Johnson, W. B. Watt, and A. H. Porter, 2014 Hybrid incompatibility arises in a sequence-based bioenergetic model of transcription factor binding. Genetics 198: 1155–1166.

Veitia, R. A., 2003 Nonlinear effects in macromolecular assembly and dosage sensitivity. J. Theor. Biol. 220: 19–25.

Veitia, R. A., S. Bottaani, and J. A. Birchler, 2013 Gene dosage effects: nonlinearities, genetic interactions, and dosage compensation. Trends Genet. 29: 385–393.

Wolfram Research, Inc., 2015 *Mathematica v10.3*. Wolfram Research, Champaign, IL.

Wray, G. A., 2007 The evolutionary significance of *cis*-regulatory mutations. Nat. Genet. 8: 206–216.

Wright, S., 1934 Physiological and evolutionary theories of dominance. Am. Nat. 68: 24–53.

Zhang, X., A. J. Cal, and J. O. Borevitz, 2011 Genetic architecture of regulatory variation in *Arabidopsis thaliana*. Genome Res. 21: 725–733.

Communicating editor: E. A. Stone

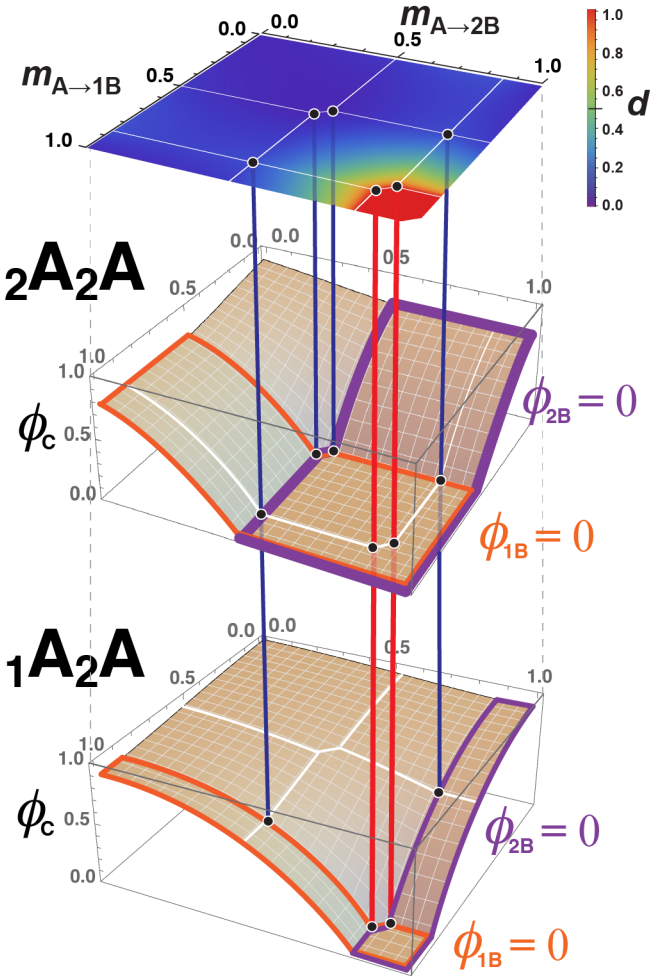

Figure S1 Genetic-background effects on dominance in the $_1A_2A \rightarrow {}_1B_2B \rightarrow CC$ case: modification of the dominance of dosage allele $_1A$ due to binding variation in the *cis* site of TF locus B. The top image is the genotype-dominance map shown in Figure 6g under conditions $[TF]_{sat} = 10$, $[_1A] = [TF]_{sat}/2$ and $[_2A] = [TF]_{sat}/10$ (detectability mask omitted), i.e., where the dosage of the $_1A$ allele is maximal and that of the $_2A$ allele is very low. Axes in this map are the binding strengths $m_{A\to 1B}$ and $m_{A\to 2B}$, i.e., binding variation in the A→B step due to variation in the *cis* site of TF locus B, and they project to the images below it. Regions separated by dotted lines in Figure 6g are here outlined in white. Projected below this map are the associated three-locus G-P maps (ϕ_C's) of the $_2A_2A$ homozygote and the $_1A_2A$ heterozygote with respect to variation at the *cis* site of TF locus B. For those genotypes, the purple lines bound the regions where $\phi_{1B} = 0$ (i.e., allele $_1B$ is not expressed in the A→B step, thus $[_1B] = 0$) and the orange lines bound the regions where $\phi_{2B} = 0$ (i.e., allele $_2B$ is not expressed in the A→B step, thus $[_2B] = 0$).

Supporting Information

Here we derive the biophysical model for text Equations 1-4, given in terms of transcription factor concentration [TF] and the dissociation constant K, from the model in Tulchinsky et al. (2014). Their version uses the absolute number of transcription factor molecules and the binding energies between a TF molecule and the promoter site to which it binds, and to competing sites the cellular and genetic background.

Parameter reduction in the biophysical model

The biophysical model we analyze is a parameter-reduced version of the model in Tulchinsky et al. (2014), developed from models of transcription-factor (TF) binding in the statistical physics literature (Gerland et al. 2002). The haploid version of that model characterizes fractional occupancy of the TF on the promoter site it regulates as

$$\theta = \frac{N'_{TF}}{N'_{TF} + \exp\left[-\Delta G + E_{diff}\right]}$$

where θ is the fractional occupancy, N'_{TF} is the absolute number of TF molecules, $-\Delta G$ (in units of $1/k_{\mathrm{B}}T$, the Boltzmann constant times the temperature in °K) is the free energy of association between a TF molecule and promoter site, and E_{diff} is the difference between the free energy of association between a TF molecule to its primary binding site and its local environmental background, which may include the non-specific binding to the genomic background as well as inhibitors and other molecules in the nuclear matrix (Mueller et al. 2013). When $E_{\mathrm{diff}} < 0$, the background is more attractive and fewer TF's are available for gene regulation; when $E_{\mathrm{diff}} > 0$, the target site is more attractive. Non-specific binding reduces the number of TF molecules in solution, making fewer available to interact with the specific binding site. We combine the E_{diff} parameter and their N'_{TF} into a single TF-availability term using $N_{\mathrm{TF}} = N'_{\mathrm{TF}}*\exp(-E_{\mathrm{diff}})$, where N_{TF} is the number of unencumbered TF molecules available for regulatory interactions, such that

$$\theta = \frac{N_{TF}}{N_{TF} + \exp\left[-\Delta G\right]}$$

Gerland et al. (2002) estimated that $E_{\mathrm{diff}} = \sim 0$ or a little less, so in practice $N_{\mathrm{TF}} = \sim N'_{\mathrm{TF}}$ unless N'_{TF} is very small.

The bioenergetic model represents the interacting TF molecules and promoter sequences as strings of bits (Figure 1a), where binding decreases with m', the number of mismatching bits (i.e., the Hamming distance between bitstrings). The second parameter modification we use is define a fractional mismatch parameter $m = m'/n$, where n is the bitstring length. Therefore, our $-\Delta G_1$ is equivalent to $-n\Delta G_1$ of Tulchinsky et al. (2014). For resolution in our density plots, we treat n as an arbitrarily large, finite integer. Reducing n would increase pixilation in those plots by averaging over blocks of area $1/n^2$, without affecting the conclusions.

Diploid model

When two allelic isoforms of a TF molecule exist, they compete for occupancy on each of the allele copies of the promoter site. Tulchinsky et al. (2014) give the diploid model as

$$\theta_{1A1\rightarrow 1B} = \frac{N_{TF.1A1}}{N_{TF.1A1} + \alpha_{2A2\rightarrow 1B}\exp\left[-m_{1A1\rightarrow 1B}\Delta G_1\right]}$$

$$\alpha_{2A2\rightarrow 1B} = 1 + N_{TF.2A2}\exp\left[m_{2A2\rightarrow 1B}\Delta G_1\right]$$

where $\theta_{1A1\rightarrow 1B}$ is the fractional occupancy of the ${}_1A_1$ isoform on the ${}_1B$ promoter site, $\alpha_{2A2\rightarrow 1B}$ is the competitive effect of binding by the ${}_2A_2$ isoform on the same ${}_1B$ promoter, $N_{\mathrm{TF.1A1}}$ and $N_{\mathrm{TF.2A2}}$ are the numbers of TF molecules of each of the isoforms that are available for binding, and $m_{1A1\rightarrow 1B}$ and $m_{2A2\rightarrow 1B}$ are the bitwise mismatches between the promoter and respective TF-isoform bitstrings. Fractional occupancies for the other three TF-promoter combinations ($\theta_{2A2\rightarrow 1B}$, $\theta_{1A1\rightarrow 2B}$ and $\theta_{2A2\rightarrow 2B}$) are calculated analogously.

Model conversion

To reach text Equation 1, substitute $[\mathrm{TF}] = N_{\mathrm{TF}}$ and $K = \exp[-\Delta G]$ and rearrange. To reach equation 2, substitute $[{}_1A_1] = N_{\mathrm{TF.1A1}}$, $[{}_2A_2] = N_{\mathrm{TF.2A2}}$ and appropriately subscripted $\Delta K^m = \exp[-m_{A\rightarrow B}\Delta G_1]$ for each of the four A→B allelic combinations, and rearrange.